

# Quench dynamics of interacting bosons: generalized coherent states versus multi-mode Glauber states

**Yulong Qiao**

Institut für Theoretische Physik, Technische Universität Dresden, D-01062 Dresden, Germany

**Frank Grossmann**

Institut für Theoretische Physik, Technische Universität Dresden, D-01062 Dresden, Germany

**Abstract.** Multi-mode Glauber coherent states (MMGS) as well as Bloch states with zero quasi-momentum, which are a special case of generalized coherent states (GCS), are frequently used to describe condensed phases of bosonic many-body systems. The difference of two-point correlators of MMGS and GCS vanishes in the thermodynamic limit. Using the established expansion of GCS in terms of MMGS, we derive a Fourier-type relation between the (auto-)correlation functions of the two different time-evolved states. This relation reveals that the (auto-)correlation and thus the dynamical free-energy density for the two cases are still different, even in the thermodynamic limit, due to the lack of the  $U(1)$  symmetry of the MMGS. Analytic results for the deep lattice model of interacting bosons for increasing filling factors show multiple sharp structures in the dynamical free energy-density of increasing complexity. These are explained using the evolution of Husimi functions in phase space.

## 1. Introduction

The dynamics of many-body quantum systems after a quench, i.e., after a slow or sudden parameter change in the Hamiltonian is at the heart of a plethora of studies in condensed matter physics and quantum information [1]. Also in cold atom physics, most experiments are based on the propagation of an initial state after the trap parameters (and thus the Hamiltonian) are suddenly or adiabatically changed, see, e.g. [2, 3, 4].

In the seminal study of Greiner et al [2], the revival dynamics of a Bose-Einstein condensate in a deep optical lattice has been investigated experimentally and described theoretically with a (multi-mode) Glauber coherent state initial condition. It has been mentioned, however, that the MMCS is only the thermodynamic limit of the true condensate ground state, described by the generalized coherent states (GCS) [5, 6, 7, 8], which is given by a product of identical single particle Bloch waves with zero quasi-momentum. Some static properties of GCS are similar to the MMCS', for example, the nonorthogonality and the impact of annihilation operators acting on them. More importantly, both states have off-diagonal long-range order, such that they are suitable to describe a Bose-Einstein condensate (BEC) [9, 10]. Nonetheless, there are distinctions between MMCS and GCS. A primary difference is that GCS maintains a definite number of particles, whereas MMCS exhibits fluctuations in particle number leading to U(1) symmetry breaking. These differences and similarities are reflected in their non-equilibrium features. The time-dependent dynamics of MMCS and GCS governed by two-body interactions has been compared in [11]. They proved that when considering the thermodynamical limit, the MMCS is equivalent to the GCS in terms of the evolution of two-point correlation function. Although the discrepancy between MMCS and GCS is not manifested in the two-point correlation case, this work will highlight the dynamical difference stemming from U(1) symmetry by examining the evolution of the autocorrelation function. The dynamics of the autocorrelation function has drawn a lot of attention, because its periodic collapse and revival in some systems is the manifestation of quantum interference [12]. More recently, the autocorrelation function is also used to study quantum dynamical phase transitions due to its analogy to the partition functions, and the transitions happens at instances of time, when the autocorrelation function is zero [13].

The use of GCS to treat the quantum dynamics of finite bosonic lattice models of Bose-Hubbard type has also been put forth more recently [14, 15, 16]. In [14], a mean-field variational approach, based on an ansatz for the solution of the time-dependent Schrödinger equation in terms of a single GCS (termed atomic coherent state) was shown to correctly predict some finite size effects in the bosonic Josephson junction (double well Bose-Hubbard system), with unsatisfactory results for more subtle quantum effects like spontaneous symmetry breaking and macroscopic self trapping, however. In [16], a multi-configuration variational approach based on GCS was taken to overcome those deficiencies. In contrast to the well-established multi-configuration time-dependent Hartree method (MCTDH) [17], the basis functions used in [16] are non-orthogonal,

such that special care has to be taken in terms of regularization of the equations of motion [18], however. This approach then led to an almost quantitative prediction also of the more elaborate quantum effects in the bosonic Josephson junction, using only a handful of basis functions, sometimes even as little as two. In addition, the fully variational approach has been shown capable of converging to the full (Fock space) quantum results for the dynamics with less computational effort and a possibly much better scaling than the factorial scaling in terms of particle and site number of the Fock space approach also for systems with more than just two wells [15].

Restricting the Hamiltonian underlying the dynamics to be separable, we will show in the following that exact results for the quantum dynamics can be gained, not only for Glauber CS but also for generalized coherent states. This is worthwhile from a mathematical standpoint but may also be helpful if benchmarks for non-separable programming and debugging tasks are asked for. Furthermore, the occurrence of sharp structures in the so-called dynamical free energy at certain points in time and their dependence on parameters like the filling factor can be studied.

The presentation is organized as follows. In Section 2, the definition of the generalized coherent states that we will frequently use as initial states is reviewed and their relation to the more commonly known Glauber or field coherent states is highlighted. In Section 3, this is followed by a review of results from the literature for the dynamics of interacting bosons in deep lattices. The focus in this section is on both, standard as well as generalized coherent state initial conditions and on the calculation of two-point correlation functions. The thermodynamic limit will then be considered, where both cases coincide. In Section 4 we go beyond charted territory by studying the relation between the (auto-)correlations and also the dynamical free-energy densities for the two different types of coherent states. It will be shown that in the thermodynamic limit, the correlations are related by a Fourier type relation. This fact is finally shown to be true also in the case of a general Hamiltonian, beyond the separable deep lattice case. Along the way, we give an explanation in terms of Husimi functions of time evolved Glauber CS for the sharp structures in the dynamic free energy. Finally, conclusions and an outlook are given and some analytical manipulations for the time evolution of a GCS are contained in the appendix.

## 2. Definition of generalized coherent states

In the following, the concept of a GCS will be reviewed along with a comprehensive discussion of its fundamental features, including a physical explanation of the state. Additionally, a key focus of this section is to highlight the relationship between generalized coherent states and the more standard, so-called Glauber CS.

As pointed out by Zhang et al [8], there exist several different kinds of GCS, which can be obtained by generalizing the concept of Glauber CS via group theory. Herein, we focus on one class of them, which are also known as  $SU(M)$  CS. The most widely

used representation of the GCS, we employ is given by [19, 20]:

$$|S, \vec{\xi}\rangle = \frac{1}{\sqrt{S!}} \left( \sum_{j=1}^M \xi_j \hat{a}_j^\dagger \right)^S |0, 0, \dots, 0\rangle, \quad (1)$$

where  $\hat{a}_j^\dagger$  represents the bosonic creation operator acting on the  $j$ -th mode or site in a lattice system and the bosonic commutator relation

$$[\hat{a}_i, \hat{a}_j^\dagger] = \delta_{ij} \quad (2)$$

is fulfilled by the ladder operators, which act on the number states as follows

$$\hat{a}|n\rangle = \sqrt{n}|n-1\rangle, \quad (3)$$

$$\hat{a}^\dagger|n\rangle = \sqrt{n+1}|n+1\rangle. \quad (4)$$

Furthermore, the ket  $|0, 0, \dots, 0\rangle$  denotes the multi-mode vacuum state, and  $S$  is the number of bosons in the GCS. The set of complex numbers  $\{\xi_j\}$  are characteristic parameters of the GCS, satisfying the normalization condition

$$\sum_{j=1}^M |\xi_j|^2 = 1, \quad (5)$$

where  $M$  is the number of different modes. The physical interpretation of  $|\xi_j|^2$  is the normalized population density or probability for the particles to be located on the  $j$ -th site. If, e.g., only a single  $\xi_j$  is one and all the others are zero, this means that all  $S$  particles are located in the  $j$ th site.

Employing the general binomial (or multinomial) theorem, a GCS can be expanded in terms of the Fock states

$$|S, \vec{\xi}\rangle = \sum_{[n_i]=S} \sqrt{S!} \prod_{i=1}^M \frac{1}{n_i!} (\xi_i \hat{a}_i^\dagger)^{n_i} |0, 0, \dots, 0\rangle, \quad (6)$$

where the sum  $\sum_{[n_i]=S}$  is the short-hand notation of  $\sum_{n_1+n_2+\dots+n_M=S}$ , which accounts for all possible configurations satisfying the constraint on the total particle number. The parameters  $S$  and  $M$  characterizing the system size determine the dimension of the Hilbert space

$$C_{M+S-1}^{M-1} = \frac{(M+S-1)!}{S!(M-1)!}, \quad (7)$$

spanned by the Fock states. This is the same as the number of possible configurations produced by placing  $S$  identical balls into  $M$  different boxes.

### 2.1. Momentum space

From the definition in Eq. (1), a GCS can be understood as a special form of condensate, where all particles macroscopically occupy a single-particle state given by  $\sum_{j=1}^M \xi_j \hat{a}_j^\dagger |0, 0, \dots, 0\rangle$ . This non-local nature of the single-particle state implies that any particle can be found at any site, with probabilities determined by  $|\xi_i|^2$ .

To further illustrate the concept of a condensate, we can represent the GCS in the

quasi-momentum frame. To this end, we consider a 1D lattice characterized by a lattice constant  $a$ . Next, we introduce a set of creation operators  $\hat{b}_k^\dagger$ , which act on the quasi-momentum  $k$ , and are related to the  $\hat{a}_j^\dagger$  through a Fourier transformation:

$$\hat{b}_k^\dagger = \frac{1}{\sqrt{M}} \sum_{j=1}^M \hat{a}_j^\dagger e^{ijk_a}, \quad (8)$$

with  $k$  ranging from  $-\frac{\pi}{a}$  to  $\frac{\pi}{a}$ . Particularly noteworthy is the case of zero quasi-momentum, for which we have

$$\hat{b}_{k=0}^\dagger = \frac{1}{\sqrt{M}} \sum_{j=1}^M \hat{a}_j^\dagger. \quad (9)$$

Homogeneous characteristic parameters of the GCS, i.e.,  $\xi_j = \frac{1}{\sqrt{M}}$  for all sites will cause all the particles to condense into the zero-momentum state

$$\frac{1}{\sqrt{S!}} \left( \sum_{j=1}^M \frac{1}{\sqrt{M}} \hat{a}_j^\dagger \right)^S |0, 0, \dots, 0\rangle = \frac{1}{\sqrt{S!}} (\hat{b}_{k=0}^\dagger)^S |0, 0, \dots, 0\rangle, \quad (10)$$

which is the so-called Bose-Einstein condensate [21].

## 2.2. Relation with multi-mode Glauber coherent states

The GCS described above exhibit a close connection with the so-called Glauber CS. For a single harmonic mode, whose Hamiltonian is given by

$$\hat{H} = \frac{\hat{p}^2}{2} + \frac{\omega^2}{2} \hat{x}^2, \quad (11)$$

the Glauber CS is defined through the action of the displacement operator on the ground state [22], and reads

$$|\alpha\rangle \equiv e^{-\frac{|\alpha|^2}{2}} e^{\alpha \hat{a}^\dagger} |0\rangle = e^{-\frac{|\alpha|^2}{2}} \sum_{n=0}^{\infty} \frac{\alpha^n}{\sqrt{n!}} |n\rangle. \quad (12)$$

As can be inferred from the definition above, a Glauber CS is an eigenstate of the annihilation operator

$$\hat{a}|\alpha\rangle = \alpha|\alpha\rangle, \quad (13)$$

where the eigenvalue  $\alpha$  is a complex number

$$\alpha = \frac{\omega^{1/2} q + i\omega^{-1/2} p}{\sqrt{2}} \quad (14)$$

in terms of the expectation values of position and momentum, denoted by  $q$ , respectively  $p$ , and also the width parameter  $\omega$ , which determines the uncertainty of position and momentum. The wavefunction of the Glauber CS in position representation is given by a Gaussian times a plane wave, according to

$$\langle x|\alpha\rangle = \left(\frac{\omega}{\pi}\right)^{\frac{1}{4}} \exp\left[-\frac{\omega}{2}(x-q)^2 + ip(x-\frac{q}{2})\right], \quad (15)$$

where the Klauder phase convention has been used [23]. For a more recent review, including further properties of Glauber CS and their use in quantum dynamics, we refer to [24].

To make contact with the GCS, the above concept has to be extended towards multi-mode Glauber CS (MMGS), represented as product states of individual single-mode Glauber CSs. As demonstrated in [19] and corroborated by the Taylor expansion of the exponential function, the MMGS denoted by  $|\vec{\alpha}\rangle = \prod_{i=1}^M |\alpha_i\rangle$ , is linked to the GCS through the following expression

$$|\vec{\alpha}\rangle = \sum_{S=0}^{\infty} \sqrt{P(S)} |S, \vec{\xi}\rangle, \quad (16)$$

with

$$P(S) = e^{-\tilde{N}} \tilde{N}^S / S!. \quad (17)$$

Here,  $\tilde{N} = \sum_{i=1}^M |\alpha_i|^2$  denotes the average number of bosons in  $|\vec{\alpha}\rangle$ . We note that the relationship between  $\xi_i$  and  $\alpha_i$  is given by

$$\xi_i = \frac{\alpha_i}{\sqrt{\tilde{N}}},$$

which is reasonable, because  $|\alpha_i|^2$  denotes the average number of particles while  $|\xi_i|^2 = \frac{|\alpha_i|^2}{\tilde{N}}$  corresponds to the normalized population density.

Furthermore, we note that if all the  $\alpha_i$  share the same phase, the corresponding GCS parameter is given by  $\xi_i = \frac{|\alpha_i|}{\sqrt{\tilde{N}}}$ , with a global ( $S$ -dependent) phase factor in front of every GCS in the sum in Eq. (16). Finally, the expression for the expansion coefficient  $P(S)$  given above proves that the total number of particles follows a Poisson distribution with the mean  $\tilde{N}$ . Eq. (16) establishes that the MMGS is a superposition of GCS with varying particle numbers  $S$ , or equivalently speaking, one GCS with particle number  $S$  can be acquired by projecting the MMGS onto the  $S$ -particle subspace. Consequently, it is natural to construct a one-to-one mapping between the GCS and MMGS.

The similarities and differences between the two sets of states are summarized in Table 1. The definitions of MMGS and GCS are presented in the second line of the table, where it becomes evident that the Glauber CS is a product state, while the GCS cannot generally be factorized. In the third line, we examine the impact of annihilation operators on the two states. The Glauber CS emerges as an eigenstate of the annihilation operator  $\hat{a}_i$  with the eigenvalue  $\alpha_i$ . In contrast,  $\hat{a}_i$  annihilates a particle from the original GCS and generates a new GCS with the particle number  $S - 1$ . Moving to the fourth line, the computation of the two-point correlation function is facilitated by the insights from the third line. The correlation functions of both states remain independent of the spatial separation between points  $i$  and  $j$ , which proves that Glauber CS and GCS have long-range phase coherence. In the next line, we present the inner product between two MMGS and two GCS, respectively, both of which are non-orthogonal. The overlap of two different MMGSs has an exponential form, and for GCS, the overlap is expressed as a polynomial.

Multi-mode Glauber CS	GCS
$ \vec{\alpha}\rangle = \prod_{i=1}^M e^{-\frac{ \alpha_i ^2}{2}} e^{\alpha_i \hat{a}_i^\dagger}  \text{vac}\rangle = \otimes_{i=1}^M  \alpha_i\rangle$	$ S, \vec{\xi}\rangle = \frac{1}{\sqrt{S!}} \left( \sum_{i=1}^M \xi_i \hat{a}_i^\dagger \right)^S  \text{vac}\rangle$
$\hat{a}_i  \vec{\alpha}\rangle = \alpha_i  \vec{\alpha}\rangle$	$\hat{a}_i  S, \vec{\xi}\rangle = \sqrt{S} \xi_i  S-1, \vec{\xi}\rangle$
$\langle \vec{\alpha}   \hat{a}_i^\dagger \hat{a}_j   \vec{\alpha} \rangle = \alpha_i^* \alpha_j$	$\langle S, \vec{\xi}   \hat{a}_i^\dagger \hat{a}_j   S, \vec{\xi} \rangle = S \xi_i^* \xi_j$
$\langle \vec{\alpha}   \vec{\beta} \rangle = \exp \left[ \sum_{i=1}^M \alpha_i^* \beta_i - \frac{1}{2} ( \alpha_i ^2 +  \beta_i ^2) \right]$	$\langle S', \vec{\xi}   S, \vec{\eta} \rangle = \left( \sum_{i=1}^M \xi_i^* \eta_i \right)^S \delta_{S, S'}$
overcomplete in whole Hilbert space	overcomplete in S-particle subspace

**Table 1.** Comparison between MMGS and GCS

### 3. Model system and dynamics

#### 3.1. Interacting-boson model

To set the stage for the investigation of the quantum dynamics of a many-body system, we first review some of the results of the seminal publication by Schachenmayer et al [11]. To this end, we consider a nonlinear Hamiltonian for interacting bosonic quantum particles, distributed over  $M$  modes (wells) of the form

$$H = \frac{U}{2} \sum_{i=1}^M \hat{a}_i^{\dagger 2} \hat{a}_i^2 = \frac{U}{2} \sum_{i=1}^M \hat{n}_i (\hat{n}_i - 1) = \sum_{i=1}^M \hat{h}_i, \quad (18)$$

where  $\{\hat{a}_i, \hat{a}_i^\dagger\}$  are the creation and annihilation operators of the previous section and  $\hat{n}_i = \hat{a}_i^\dagger \hat{a}_i$  is the corresponding number operator. Furthermore,

$$\hat{h}_i = \frac{U}{2} \hat{n}_i (\hat{n}_i - 1) \quad (19)$$

stands for the local Kerr-type Hamiltonians with on-site interaction strength  $U$ . The total Hamiltonian is the limiting case of vanishing hopping strength of the Bose-Hubbard model and can be realized in experiment by increasing the intensity of the optical lattice laser beams [2].

#### 3.2. Two-point correlation function for Glauber as well as generalized coherent states

Other dynamical quantities that are frequently studied in the literature are the auto-correlation [2, 25] as well as the two-point correlation function (TPCF) [11]. In the following, we focus on the two-point correlation and postpone the discussion of the auto-correlation to Sec. 4.

The analytical results to be derived for the cases of MMGS and GCS provide an insight for the connection between these two types of states. First, we revisit the results from [11], as their findings offer a comprehensive understanding of the relationship

between the dynamics of Glauber as well as generalized coherent states. We also provide a more concise derivation for the case of GCS than the one in [11], by using some of the properties listed in Table. 1.

In the deep-lattice case, the two-point correlation function of a MMGS can be derived as follows [11]

$$\begin{aligned}
 \langle \vec{\alpha} | e^{i\hat{H}t} \hat{a}_i^\dagger \hat{a}_j e^{-i\hat{H}t} | \vec{\alpha} \rangle &= \langle \alpha_i | \langle \alpha_j | e^{i(\hat{h}_i + \hat{h}_j)t} \hat{a}_i^\dagger \hat{a}_j e^{-i(\hat{h}_i + \hat{h}_j)t} | \alpha_i \rangle | \alpha_j \rangle \\
 &= \langle \alpha_i | e^{i\hat{h}_i t} \hat{a}_i^\dagger e^{-i\hat{h}_i t} | \alpha_i \rangle \langle \alpha_j | e^{i\hat{h}_j t} \hat{a}_j e^{-i\hat{h}_j t} | \alpha_j \rangle \\
 &= \langle \alpha_i | \hat{a}_i^\dagger e^{iU\hat{n}_i t} | \alpha_i \rangle \langle \alpha_j | e^{-iU\hat{n}_j t} \hat{a}_j | \alpha_j \rangle \\
 &= \alpha_i^* \alpha_j \langle \alpha_i | \alpha_i e^{iUt} \rangle \langle \alpha_j | \alpha_j e^{-iUt} \rangle \\
 &= \alpha_i^* \alpha_j \exp [|\alpha_i|^2 (e^{iUt} - 1)] \exp [|\alpha_j|^2 (e^{-iUt} - 1)] \\
 &= |\alpha|^2 e^{2|\alpha|^2 [\cos(Ut) - 1]}
 \end{aligned} \tag{20}$$

where in the third line, we have used the formulas  $\hat{a}_k f(\hat{n}_k) = f(\hat{n}_k + 1) \hat{a}_k$  and  $\hat{a}_k^\dagger f(\hat{n}_k) = f(\hat{n}_k - 1) \hat{a}_k^\dagger$ , and we obtain the result in the fourth line via the fact

$$e^{i\varphi \hat{n}_k} | \alpha_k \rangle = \sum_{n=0}^{\infty} \frac{\alpha_k^n}{\sqrt{n!}} e^{i\varphi n} | n \rangle_k = | \alpha_k e^{i\varphi} \rangle. \tag{21}$$

For the last line, the system is assumed to be homogeneous:  $\alpha_i = \alpha_j = \alpha$ . From the final result, it is clear that the evolution of the correlation function is also driven by the on-site interaction effect, exhibiting a periodic behavior with a period of  $2\pi/U$ .

As proposed in [11], we now choose the GCS defined in Eq. (1) as the initial state. Physically, this choice appears more reasonable compared to the Glauber CS, given the fact that the ground state of a definite number of particles for the nearest-neighbor hopping model with periodic boundary conditions

$$\hat{H}_{\text{NN}} = - \sum_{\langle i,j \rangle} t_{i,j} \hat{a}_i^\dagger \hat{a}_j \tag{22}$$

i.e., a Bose-Hubbard Hamiltonian, where only the hopping term with amplitudes  $t_{ij}$  is present, is described by a GCS [11, 26]. The particular setup to be studied in the following thus corresponds to a quench dynamics: the lattice is initially shallow where particles can move freely among different sites, and the system is prepared in the ground state. At  $t = 0$  the lattice is abruptly deepened as shown schematically in Fig. 1, so the initial state which is no longer an eigenstate will start to evolve.



**Figure 1.** Transition from the shallow lattice (almost free boson model) to deep lattice (on-site interaction only).

The dynamics of the two-point correlation function of an initial GCS governed by the



interacting boson Hamiltonian of Eq. (18) is given as follows:

$$\begin{aligned}
 \langle S, \vec{\xi} | e^{i\hat{H}t} \hat{a}_i^\dagger \hat{a}_j e^{-i\hat{H}t} | S, \vec{\xi} \rangle &= \langle S, \vec{\xi} | e^{i(\hat{h}_i + \hat{h}_j)t} \hat{a}_i^\dagger \hat{a}_j e^{-i(\hat{h}_i + \hat{h}_j)t} | S, \vec{\xi} \rangle \\
 &= \langle S, \vec{\xi} | \hat{a}_i^\dagger e^{iU\hat{n}_i t} e^{-iU\hat{n}_j t} \hat{a}_j | S, \vec{\xi} \rangle \\
 &= S \xi_i^* \xi_j \langle S-1, \vec{\xi} | e^{iU\hat{n}_i t} e^{-iU\hat{n}_j t} | S-1, \vec{\xi} \rangle \\
 &= S \xi_i^* \xi_j \left( |\xi_i|^2 e^{iUt} + |\xi_j|^2 e^{-iUt} + \sum_{k \neq i, j}^M |\xi_k|^2 \right)^{S-1}, \quad (23)
 \end{aligned}$$

where we have used the intermediate result

$$\begin{aligned}
 e^{i\varphi \hat{n}_k} | S, \vec{\xi} \rangle &= e^{i\varphi \hat{n}_k} \frac{1}{\sqrt{S!}} \left( \sum_{i=1}^M \xi_i \hat{a}_i^\dagger \right)^S | \text{vac} \rangle \\
 &= \sum_{[n_i]=S} \frac{S!}{n_1! n_2! \dots n_M!} e^{i\varphi \hat{n}_k} (\xi_1 a_1^\dagger)^{n_1} \dots (\xi_k a_k^\dagger)^{n_k} \dots (\xi_M a_M^\dagger)^{n_M} | \text{vac} \rangle \\
 &= \sum_{[n_i]=S} \frac{S!}{n_1! n_2! \dots n_M!} (\xi_1 a_1^\dagger)^{n_1} \dots (\xi_k a_k^\dagger)^{n_k} \dots (\xi_M a_M^\dagger)^{n_M} e^{i\varphi(\hat{n}_k + n_k)} | \text{vac} \rangle \\
 &= \sum_{[n_i]=S} \frac{S!}{n_1! n_2! \dots n_M!} (\xi_1 \hat{a}_1^\dagger)^{n_1} \dots (\xi_k e^{i\varphi} \hat{a}_k^\dagger)^{n_k} \dots (\xi_M \hat{a}_M^\dagger)^{n_M} e^{i\varphi(\hat{n}_k + n_k)} | \text{vac} \rangle \\
 &= | S, \vec{\xi} \rangle, \quad (24)
 \end{aligned}$$

where  $\vec{\xi} = \{\xi_1, \xi_2, \dots, \xi_k e^{i\varphi}, \dots, \xi_M\}$ ,  $\langle S, \vec{\xi} | S, \vec{\xi} \rangle = (|\xi_k|^2 e^{i\varphi} + \sum_{i \neq k}^M |\xi_i|^2)^S$ . This result illustrates that the effect of the number operator  $\hat{n}_j$  is to imprint a phase factor on the  $j$ -th site, similar to the case of Glauber CS displayed in Eq. (21). We note that the result in Eq. (23) can also be obtained with the help of projection operator techniques [11].

For the special case where  $i = j$ , the correlation function simplifies to

$$\begin{aligned}
 \langle S, \vec{\xi} | e^{i\hat{H}t} \hat{a}_i^\dagger \hat{a}_i e^{-i\hat{H}t} | S, \vec{\xi} \rangle &= \langle S, \vec{\xi} | e^{i\hat{h}_i t} \hat{a}_i^\dagger \hat{a}_i e^{-i\hat{h}_i t} | S, \vec{\xi} \rangle \\
 &= \langle S, \vec{\xi} | \hat{a}_i^\dagger \hat{a}_i | S, \vec{\xi} \rangle \\
 &= S |\xi_i|^2 \quad (25)
 \end{aligned}$$

For simplicity, we consider the homogeneous state  $\xi_1 = \xi_2 = \dots = \xi_M = \frac{1}{\sqrt{M}}$ , which corresponds to the zero quasi-momentum state of Eq. (9). Under this condition, the correlation function Eq. (23) simplifies to

$$\langle \hat{a}_i^\dagger \hat{a}_j \rangle = \frac{S}{M} \left[ 1 + \frac{2}{M} \cos(Ut) - \frac{2}{M} \right]^{S-1} \quad (26)$$

In the thermodynamic limit,  $S \rightarrow \infty$ ,  $M \rightarrow \infty$  with finite filling factor

$$\lambda = \frac{S}{M}, \quad (27)$$

Eq. (23) converges to

$$\begin{aligned}
 \lim_{S \rightarrow \infty} \langle \hat{a}_i^\dagger \hat{a}_j \rangle &= \lim_{S \rightarrow \infty} \frac{S}{M} \left[ 1 + \frac{S}{M} \frac{2}{S} \cos(Ut) - \frac{S}{M} \frac{2}{S} \right]^{S-1} \\
 &= \lambda e^{\lambda[-2+2\cos(Ut)]}. \quad (28)
 \end{aligned}$$

The similarity between Eq. (20) and Eq. (28) reveals that the relationship between Glauber CS and GCS can be established by setting  $\alpha = \sqrt{\lambda}$ , which is also corroborated by Eq. (16). This demonstrates that the correlation function of GCS is identical to that of the Glauber CS in the thermodynamic limit. As proven in [11], this identity is achieved already for rather small values of  $S$ .

#### 4. Auto-correlation function of the evolved GCS

Although GCS and Glauber CS share similarities for dynamical quantities like the two-point correlation functions and thus also the quasi-momentum distribution, differences between them still exist, even in the thermodynamic limit. To prove this fact, we will investigate the time-dependent auto-correlation function of the GCS in the following and express the result in terms of a related quantity for MMGS.

##### 4.1. Dynamical free energy density

Given the similarity between the auto-correlation function

$$\langle \Psi(0) | e^{-i\hat{H}t} | \Psi(0) \rangle \quad (29)$$

and the partition function in equilibrium statistical mechanics

$$Z = \text{tr}(e^{-\beta\hat{H}}) = e^{-\beta Nf}, \quad (30)$$

where  $\beta = 1/kT$  is proportional to the inverse of temperature,  $N$  denotes the number of degrees of freedom and  $f$  is the free-energy density, an analog of thermodynamic phase transitions, i.e., a nonanalytic behaviour at critical times in quantum dynamics was predicted [13, 27, 28, 29].

In the following, we consider the dynamical free energy, defined by

$$\mathcal{L} \equiv -\frac{1}{M} \log(|\langle \Psi(0) | \Psi(t) \rangle|^2), \quad (31)$$

where the initial state in our case

$$|\Psi(0)\rangle = |S, \vec{\xi}\rangle \quad (32)$$

is the GCS with homogeneous parameters. As proven in the appendix, the auto-correlation function (or Loschmidt amplitude) is then given by

$$\langle \Psi(0) | \Psi(t) \rangle = \langle S, \vec{\xi} | e^{-i\hat{H}t} | S, \vec{\xi} \rangle = S! \sum_{[n_i]=S} \prod_{i=1}^M \frac{|\xi_i|^{2n_i}}{n_i!} e^{-i\frac{U}{2}n_i^2 t} \quad (33)$$

and thus the dynamical free energy density [30] is, at least in principle, at our disposal.

Although the summation in Eq. (33) has no obvious closed solution for  $U \neq 0$ , the numerical solution is accessible, however, via the concept of generating functions [31, 32] that allows for a relatively straightforward evaluation of the restricted summation in Eq. (33), which would otherwise be impossible to tackle, already for moderate particle and site numbers. The general idea of the generating function method is to design a polynomial in the variable  $x$  with the constraint that the coefficient for

the term  $x^S$  is related to Eq. (33). This method turns the problem into calculating the polynomial coefficients which can be done by efficient convolution algorithm. For instance, if the generating function is the product of two polynomials, represented as  $(\sum_{i=1}^{\infty} a_i x^i) (\sum_{j=1}^{\infty} b_j x^j)$ , the coefficient in front of the  $x^n$  can be expressed as

$$\sum_{i=1}^{\infty} a_i b_{n-i},$$

which is the convolution between two series with coefficients  $\{a_i\}$  and  $\{b_i\}$ .

Let us first consider the homogeneous situation  $\xi_1 = \xi_2 = \dots = \xi_M = \frac{1}{\sqrt{M}}$ , simplifying Eq. (33) to

$$\langle S, \vec{\xi} | e^{-i\hat{H}t} | S, \vec{\xi} \rangle = \frac{S!}{M^S} \sum_{[n_i]=S} \prod_{i=1}^M \frac{1}{n_i!} e^{-i\frac{U}{2} n_i^2 t} \quad (34)$$

We define a polynomial

$$F(x) = \left[ \sum_{k=0}^M \phi(k) x^k \right]^M, \quad \phi(k) = \frac{e^{-i\frac{U}{2} k^2 t}}{k!} \quad (35)$$

which plays the role of generating function, so the result in Eq. (34) is given by  $\frac{S!}{M^S} [x^S] F(x)$ , where  $[x^S] F(x)$  denotes the coefficient for term  $x^S$  in the polynomial  $F(x)$ . In the general situation, a series of independent polynomials are needed

$$\tilde{F}(x) = f_1(x) f_2(x) \dots f_M(x), \quad f_i(x) = \sum_{k=0}^M \frac{|\xi_i|^{2k} e^{-i\frac{U}{2} k^2 t}}{k!} x^k \quad (36)$$

and Eq. (33) is given by  $S! [x^S] \tilde{F}(x)$ .

For the plot in Fig. 2, we fix the value of the particle number to  $S = 100$  and vary the ratio  $\lambda = \frac{S}{M}$  to investigate the dynamics. From Fig. 2, we can observe that for large values of  $\lambda$ , the dynamical free-energy density has several peaks within one period. As  $\lambda$  is decreased, these peaks gradually disappear, leaving just one peak occurring at  $Ut = \pi$  when  $\lambda = 0.5$ . Due to the definition of the dynamical free-energy density in Eq. (31), these peaks correspond to the local minima of the survival probability. When the survival probability completely vanishes, non-analytical kinks appear in the curves. This phenomenon is recognized as a quantum dynamical phase transition (QDPT) in the literature [33, 34, 35]. The authors in [30] have studied the QDPT of the non-equilibrium dynamics induced by the quench from the superfluid phase to the Mott-insulator phase present in the full Bose-Hubbard model, whereas in [36], kink-like features in the rate function have been shown to exist in a dissipative model of quantum optics (Dicke model) already at moderate particle number.

In order to gain some understanding of the peak structure seen in Fig. 2, we will now elucidate the connection of the auto-correlation with the one in the MMGS case, given by

$$\begin{aligned} \langle \vec{\alpha} | e^{-i\hat{H}t} | \vec{\alpha} \rangle &= \otimes_{i=1}^M \langle \alpha_i | \exp(-i\hat{h}_i t) | \alpha_i \rangle \\ &= \prod_{i=1}^M e^{-|\alpha_i|^2} \sum_{n_i=0}^{\infty} \frac{|\alpha_i|^{2n_i}}{n_i!} e^{-i\frac{U}{2} n_i(n_i-1)t}. \end{aligned} \quad (37)$$

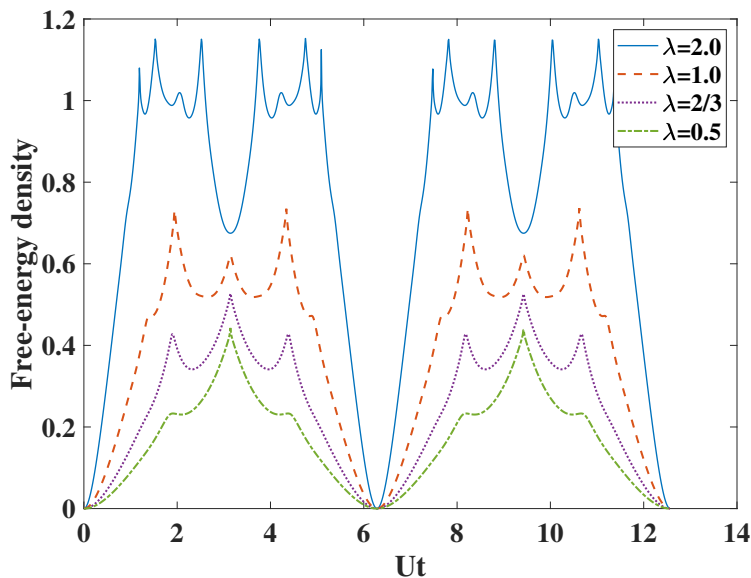


**Figure 2.** Dynamical free-energy density for GCS initial condition as a function of time  $Ut$ , ranging from 0 to  $4\pi$ . The total number of particles is  $S = 100$  and results are shown for different values of filling factor  $\lambda = S/M$

This result is factorized and does not impose constraints on the total number of particles and is thus very easily accessible to numerical treatment. The corresponding free-energy density for the case of filling factor  $\lambda = 2$  is depicted by the solid line in Fig. 3 and shows a similar peak structure with minima at  $Ut$  equal to integer multiples of  $2\pi$  as above. The corresponding classical result (starting from the same quantum mechanical initial condition), calculated using the truncated Wigner approximation is comparatively structureless, as displayed by the dashed line. The peaks can thus be considered as quantum effects.

To make use of the simple form of the auto-correlation in the Glauber case, we are looking for a relation between the two cases. To find this relation, we introduce an irrelevant phase and rewrite the homogeneous GCS auto-correlation given in Eq. (33) as follows:

$$\begin{aligned}
 \langle S, \vec{\xi} | e^{-i\hat{H}t} | S, \vec{\xi} \rangle &= S! \sum_{[n_i]=S} \prod_{i=1}^M \frac{1}{n_i!} \frac{1}{M^{n_i}} e^{-i\frac{U}{2} n_i (n_i - 1)t} \\
 &= S! \sum_{n_1=0}^{\infty} \sum_{n_2=0}^{\infty} \cdots \sum_{n_M=0}^{\infty} \delta_{S, \sum_{i=1}^M n_i} \prod_{i=1}^M \frac{1}{n_i!} \frac{1}{M^{n_i}} e^{-i\frac{U}{2} n_i (n_i - 1)t} \\
 &= S! \sum_{n_1=0}^{\infty} \sum_{n_2=0}^{\infty} \cdots \sum_{n_M=0}^{\infty} \int_0^1 dx e^{-i2\pi x (S - \sum_{i=1}^M n_i)} \prod_{i=1}^M \frac{1}{n_i!} \frac{1}{M^{n_i}} e^{-i\frac{U}{2} n_i (n_i - 1)t} \\
 &= S! \sum_{n_1=0}^{\infty} \sum_{n_2=0}^{\infty} \cdots \sum_{n_M=0}^{\infty} \int_0^1 dx e^{-i2\pi x S} \prod_{i=1}^M \frac{1}{n_i!} \frac{1}{M^{n_i}} e^{-i\frac{U}{2} n_i (n_i - 1)t + i2\pi x n_i}
 \end{aligned}$$

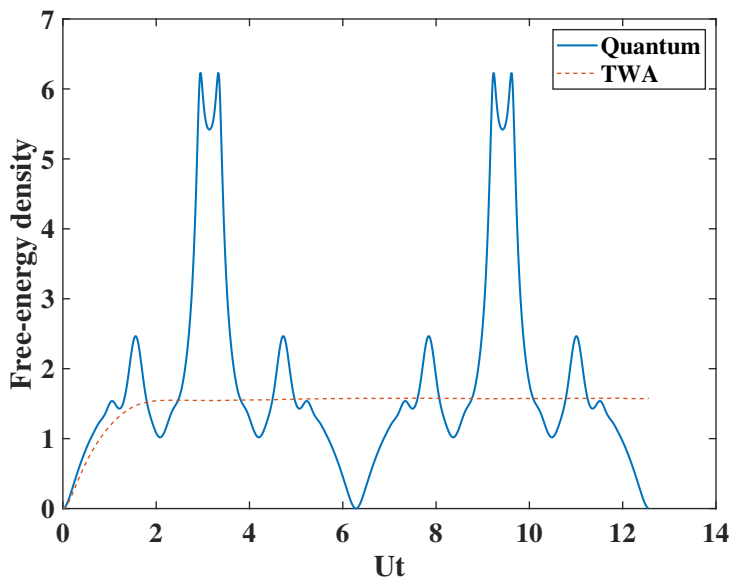


**Figure 3.** Dynamical free-energy density for a Glauber state initial condition as a function of time  $Ut$ , ranging from 0 to  $4\pi$ . The filling factor is  $\lambda = 2$ . Solid line: full quantum result; dashed line: TWA result

$$\begin{aligned}
 &= S! \int_0^1 dx e^{-i2\pi x S} \left( \sum_{n=0}^{\infty} \frac{1}{n!} \frac{1}{M^n} e^{-i\frac{U}{2}n(n-1)t + i2\pi x n} \right)^M \\
 &= \frac{S!}{S^S} \int_0^1 dx e^{-i2\pi x S} \left( \sum_{n=0}^{\infty} \frac{1}{n!} \frac{S^n}{M^n} e^{-i\frac{U}{2}n(n-1)t + i2\pi x n} \right)^M, \tag{38}
 \end{aligned}$$

where in the first line, the global phase factor  $e^{i\frac{U}{2}St} = e^{i\frac{U}{2}\sum_{i=1}^M n_i t}$  is incorporated, in order to ease the comparison with the Glauber CS case. In the second line the Kronecker symbol  $\delta_{S, \sum_{i=1}^M n_i}$  is introduced to impose the constraint on the total particle number and meanwhile lift the restriction on the particle number of the single mode. The third line follows by replacing the Kronecker symbol with an integral

$$\delta_{S, \sum_{i=1}^M n_i} = \int_0^1 dx e^{-i2\pi x (S - \sum_{i=1}^M n_i)}. \tag{39}$$

Furthermore, by incorporating the factor  $\frac{S!}{S^S}$  into the bracket, we are able to define the function

$$G(x, t) = \left[ \sum_{n=0}^{\infty} \frac{1}{n!} \left( \frac{S!}{S^S} \right)^{1/M} \frac{S^n}{M^n} e^{-i\frac{U}{2}n(n-1)t + i2\pi x n} \right]^M \tag{40}$$

that will play a central role.

Further progress can now only be made in the limit of large particle numbers, because in this case, we are able to use Stirling's approximation  $S! \approx \sqrt{2\pi S} \left(\frac{S}{e}\right)^S$  of the factorial to simplify the factor  $\left(\frac{S!}{S^S}\right)^{1/M}$  as

$$\left(\frac{S!}{S^S}\right)^{1/M} \approx \sqrt[2M]{2\pi S} \left(\frac{S}{Se}\right)^{\frac{S}{M}}, \tag{41}$$

Combining Eq. (38), Eq. (40) and Eq. (41), we have

$$\langle S, \vec{\xi} | e^{-i\hat{H}t} | S, \vec{\xi} \rangle = \sqrt{2\pi S} \int_0^1 dx e^{-i2\pi x S} G(x, t) \quad (42)$$

where the  $G(x, t)$  is expressed alternatively as

$$G(x, t) = \left[ \sum_{n=0}^{\infty} \frac{\lambda^n e^{-\lambda}}{n!} e^{-i\frac{U}{2}n(n-1)t + i2\pi x n} \right]^M. \quad (43)$$

Inspired by the form of Eq. (42), we interpret the survival probability amplitude of the time-evolved GCS as the Fourier coefficient of  $G(x, t)$  at a specific "frequency" denoted by  $S$  ‡.

By comparing Eqs. (43) and (37), we observe that the function  $G(x, t)$  is the cross-correlation of two different MMGS, i.e.,

$$G(x, t) = \langle \vec{\alpha}' | e^{-i\hat{H}t} | \vec{\alpha} \rangle, \quad (44)$$

where  $|\vec{\alpha}\rangle$  is a multimode Glauber CS with  $\alpha_i = \sqrt{\lambda}$  for  $\forall i$ , and  $|\vec{\alpha}'\rangle$  is a similar CS with a phase shifted parameter, characterized by

$$\alpha'_j = \sqrt{\lambda} e^{-i2\pi x} \quad (45)$$

for  $\forall j$  with

$$0 \leq x < 1. \quad (46)$$

Despite the phase shift,  $|\vec{\alpha}\rangle$  and  $|\vec{\alpha}'\rangle$  are expanded by the same GCS as discussed below Eq. (16). Essentially, this phase shift is rooted in the  $U(1)$  symmetry (conservation of particle number) of the GCS, which the Glauber CS do not obey. Another significant insight gained from Eq. (42) is that if the value of  $G(x)$  is zero, the survival probability will consequently be zero as well.

Before we continue the discussion of the dynamical free-energy density a few remarks are in order: The generating function approach helps to get a numerical handle on the calculation of the GCS auto-correlation in the case of the Bose-Hubbard model with onsite interaction only. It will, however, not be generalizable to the dynamics including inter-site hopping. In contrast, the Fourier relation between the GCS auto-correlation and the cross-correlation of the Glauber coherent state (which is just a direct product in the deep lattice case), although it is derived for large particle numbers, is more general in terms of the Hamiltonians, it can be used for, as will be further elucidated below.

*4.1.1. Thermodynamic limit* To be specific, we consider the case of unit filling factor  $\lambda = 1$ , which corresponds to the thermodynamic limit when both  $S$  and  $M$  are large and equal. In this case, the function§

$$G(x, t) = \left[ \sum_{n=0}^{\infty} \frac{e^{-1}}{n!} e^{-i\frac{U}{2}n(n-1)t + i2\pi x n} \right]^M \quad (47)$$

‡ We note that the Fourier-transform pair of variables in the present case are  $x$  and  $S$

§ This function is similar to the (finite) Jacobi theta sums studied in [37] in the context of quantum carpets but is more complex due to the presence of the factorial term as well as the infinite summation

represents the overlap function of the time-evolved MMGS  $e^{-i\hat{H}t}|\vec{\alpha}\rangle$  with MMGS distributed along the unit circle in phase space.

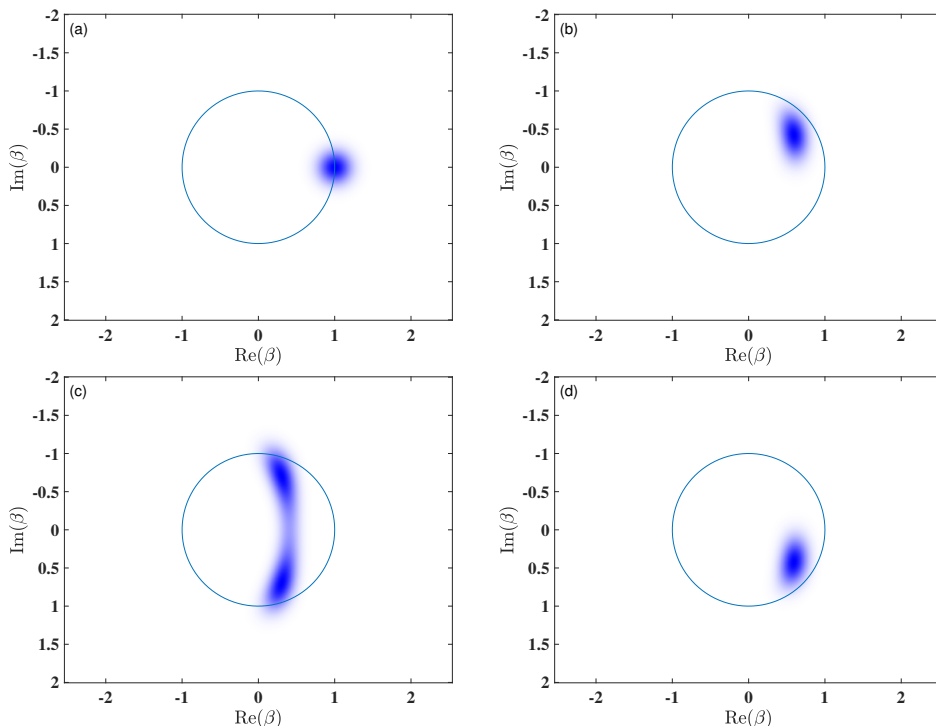


**Figure 4.** The distribution function  $|\langle\beta|e^{-i\hat{H}t}|\alpha\rangle|^M$  in phase space  $(\text{Re}(\beta), \text{Im}(\beta))$  at different points in time: (a)  $Ut = 0$ , (b)  $Ut = \frac{\pi}{2}$ , (c)  $Ut = \pi$  and (d)  $Ut = \frac{3\pi}{2}$ . The characteristic CS parameter is  $\alpha = 1$  and the system parameter is  $M = 50$ .

In Fig. 4, we present the dynamics of the function  $|\langle\beta|e^{-i\hat{H}t}|\alpha\rangle|^M$  with the single site cross-correlation

$$c_{\beta\alpha}(t) \equiv \langle\beta|e^{-i\hat{H}t}|\alpha\rangle = \exp\left[-\frac{|\alpha|^2 + |\beta|^2}{2}\right] \sum_{n=0}^{\infty} \frac{(\alpha\beta^*)^n}{n!} e^{-i\frac{U}{2}n(n-1)t} \quad (48)$$

for system size  $S = M = 50$ . The value of  $|G(x, t)|$  is determined by the distribution of  $|\langle\beta|e^{-i\hat{H}t}|\alpha\rangle|^M$  on the unit circle. It can be inferred that this function evolves around the origin, and the value of  $|G(x, t)|$  is significantly influenced by the spot's relative position to the circle. Pictorially, when the circle does not intersect the center of the spot, the survival probability decreases, leading to the emergence of sharp structures in the rate function at these points in time. Moreover, as  $M$  approaches infinity, the shape of the spot shrinks into a point, indicating that once the center of the point leaves the circle, the survival probability rapidly drops towards zero. Furthermore, we stress that in the present case, the distribution function displayed in Fig. 4, at no instance in time is attaining appreciable weight for negative real part of  $\beta$  in contrast to the case of larger values of  $\lambda$  to be discussed below.

Finally, let us study the influence of the shape of the spot. For example, when  $\lambda$  is large the spot tends to split into two parts when  $Ut = \pi$ , possibly introducing extra intersections with the circle, as displayed in Fig. 4 (c). Conversely, if  $\lambda$  is small such

as the case  $\lambda = \frac{2}{3}$ , the spot will maintain its shape and the center remains distanced from the circle at  $Ut = \pi$  displayed in Fig. 5, resulting in the gradual dominance of the central peak at  $Ut = \pi$  for decreasing  $\lambda$  as shown in Fig. 2.

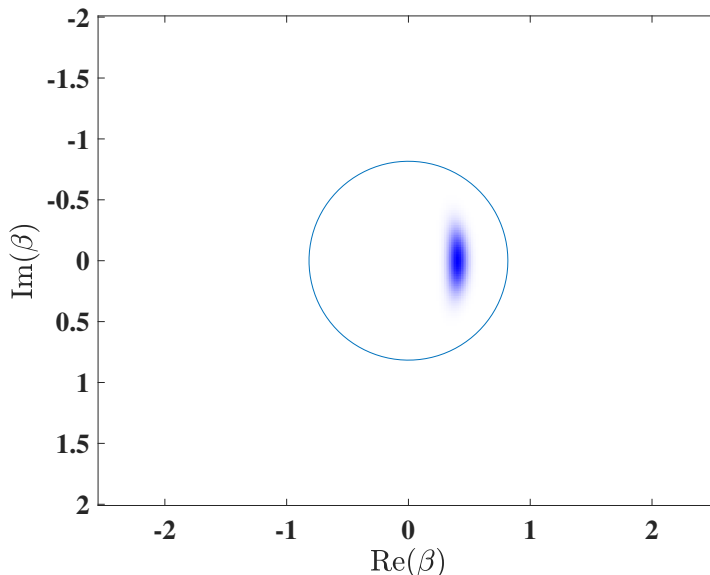


**Figure 5.** The distribution function  $|\langle \beta | e^{-i\hat{H}t} | \alpha \rangle|^M$  for  $\lambda = \frac{2}{3}$  with  $S = 100$  at  $Ut = \pi$ .

*4.1.2. The case of large filling factor* Another noteworthy scenario occurs when  $S \gg M$ , where the Eq. (42) still holds. However, the underlying distribution in phase space and the corresponding free-energy density are much more complicated. In contrast to the results in Fig. 2, the free-energy density in Fig. 6 for  $S = 100$  and  $M = 3$  contains more peaks, especially two pronounced spikes located around  $x = 2.074$  and  $x = 4.2$  within the first period. These peaks are associated with the local or global minimal values of the survival probability.

In Fig. 7, the corresponding distribution function  $|\langle \beta | e^{-i\hat{H}t} | \alpha \rangle|^M$  for  $\alpha = \sqrt{\lambda} = \sqrt{\frac{100}{3}}$  is depicted. This distribution splits into several spots which form multi-component cat states at different instances of time. To gain some insight, let us focus on the result at the instance  $Ut = \pi$ , displayed in panel (f). The cross-correlation from Eq. (49) then reads

$$\begin{aligned} c_{\beta\alpha}(\pi/U) &= \exp\left[-\frac{|\alpha|^2 + |\beta|^2}{2}\right] \sum_{n=0}^{\infty} \frac{(\alpha\beta^*)^n}{n!} e^{-i\frac{\pi}{2}n(n-1)} \\ &= \exp\left[-\frac{|\alpha|^2 + |\beta|^2}{2}\right] \sum_{n=0}^{\infty} \frac{(\alpha\beta^* e^{-i\frac{\pi}{2}(n-1)})^n}{n!} \end{aligned} \quad (49)$$

and we consider the cases of purely imaginary  $\beta_{\pm} = |\beta|e^{\pm i\pi/2}$ , when the term under the  $n$ -th power becomes  $\pm\alpha|\beta|e^{-in\pi/2}$ . Now using Euler's formula  $e^{-in\pi/2} = \cos(n\pi/2) -$



$i \sin(n\pi/2)$ , we realize that the summation over  $n$  can be brought into closed form according to

$$\sum_{n=0}^{\infty} \frac{(\alpha\beta^* e^{-i\frac{\pi}{2}(n-1)})^n}{n!} = \cosh(\alpha|\beta|) \mp i \sinh(\alpha|\beta|) \quad (50)$$

and for  $\alpha = |\beta| \gg 1$ , we get

$$c_{\beta\alpha}(\pi/U) \approx \frac{1}{2} \mp \frac{i}{2}. \quad (51)$$

Away from the center of the two spots in panel (f) of Fig. 7, the cross-correlation and thus the distribution function will be exponentially suppressed. For different special times, as shown in the other panels of Fig. 7, there may be more of those spots, all of which move along the circle with radius  $\sqrt{\lambda}$ , however, as the quantum fluctuation of the Glauber CS with large  $\alpha$  is suppressed. Consequently, the vanishing of the survival probability can not be attributed to the deviation of  $G(x, t)$  from the circle, as it was possible before.

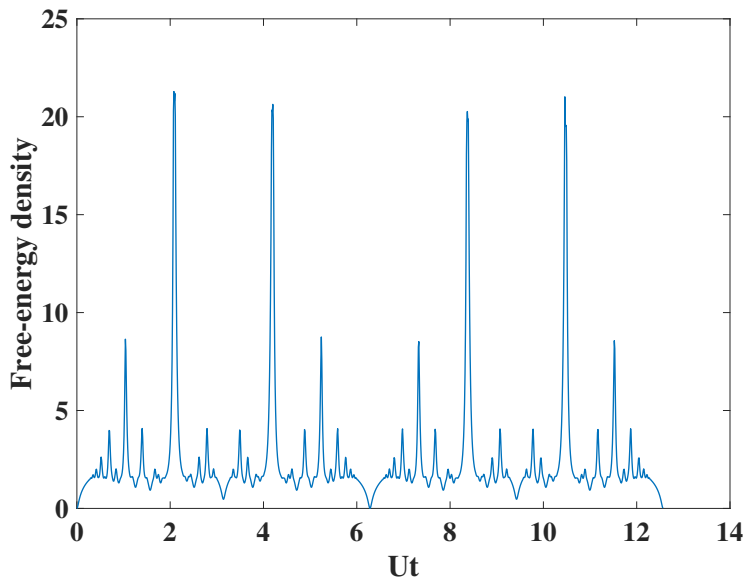


**Figure 6.** Dynamical free-energy density as a function of time  $Ut$  ranging from 0 to  $4\pi$ . The system size is set to be  $S = 100$  and  $M = 3$ .

Instead, we should examine the integrand on the right hand side of Eq. (42)

$$F(x, t) = e^{-i2\pi x S} G(x, t). \quad (52)$$

In Fig. 8, we divide the  $F(x, t)$  into real and the imaginary parts, and choose two typical times to observe how they vary with  $x$ , ranging from 0 to 1. In the left figure, the time is fixed at  $Ut = \frac{\pi}{2}$  corresponding to Fig. 7 (d) where the four spots manifest as four peaks. Because three peaks are negative and one is positive, all of them displaying similar heights, the integral of the real part with respect to the  $x$  is not zero resulting in a finite survival probability. In the right figure, however, the time is selected to be  $Ut = 2.074$  identical with the position of the first main spike in Fig. 6. In this case, the

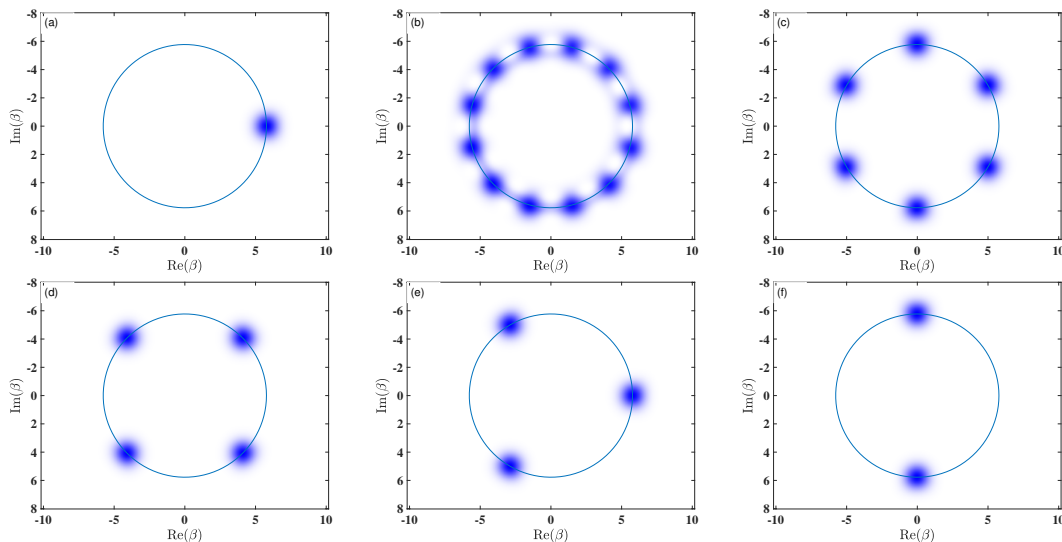


**Figure 7.** The distribution function  $|\langle\beta|\alpha\rangle|^M$  with  $M = 3$  in phase space  $(\text{Re}(\beta), \text{Im}(\beta))$  at different times: (a)  $Ut = 0$ , (b)  $Ut = \frac{\pi}{6}$ , (c)  $Ut = \frac{2\pi}{6}$ , (d)  $Ut = \frac{3\pi}{6}$ , (e)  $Ut = \frac{4\pi}{6}$  and (f)  $Ut = \pi$ . The characteristic CS parameter is  $\alpha = \sqrt{\frac{100}{3}}$ .

integral of both real and imaginary components is very small, since the peaks manifest as either positive or negative. The contributions with opposing signs ultimately cancel each other out, giving rise to the decrease of the overall integral. As a result, the survival probability will also go towards zero. In summary, when  $\lambda$  is large, the value of the survival probability depends on the collective effects of all the spots.

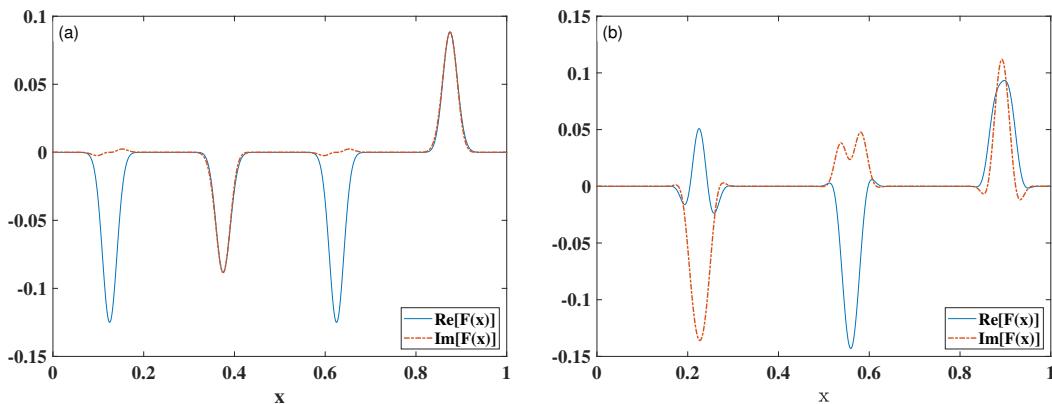


**Figure 8.** The real part (solid blue) and the imaginary part (read dot-dash) of the  $F(x, t)$  as the function of  $x$  for two fixed time points: (a)  $Ut = \frac{\pi}{2}$  and (b)  $Ut = 2.074$ . The system parameters are same with ones in Fig. 7.

#### 4.2. General Hamiltonian

The connection between the auto-correlations of the different types of CS that we have just established can be generalized to a generic but number conserving Hamiltonian  $\hat{H}$ .

A commonly used example would, e.g., be the Bose-Hubbard Hamiltonian, containing the on-site interaction, we have considered so far as well as an inter-site hopping term, see, e.g., Eq. (22). To proceed, we recall Eq. (16) and expand the survival amplitude of the Glauber CS as

$$\langle \vec{\alpha} | e^{-i\hat{H}t} | \vec{\alpha} \rangle = e^{-\tilde{N}} \sum_{S'=0}^{\infty} \frac{\tilde{N}^{S'}}{S'!} \langle S', \vec{\xi} | e^{-i\hat{H}t} | S', \vec{\xi} \rangle. \quad (53)$$

The next step is to extract the term  $\langle S', \vec{\xi} | e^{-i\hat{H}t} | S', \vec{\xi} \rangle$  from the sum. An elegant way to perform this task is to utilize the projection operator onto a specific particle number  $S$ , as defined in [11]

$$\hat{P} = \int_0^1 dx e^{i2\pi x(\hat{N}-S)} \quad (54)$$

where  $\hat{N} = \sum_{i=1}^M a_i^\dagger \hat{a}_i$ . It is clear that the operator  $\hat{P}$  plays the role of  $\delta_{S',S}$ .

Applying the operator  $\hat{P}$  to both sides of Eq. (53), we get

$$\begin{aligned} & \int_0^1 dx e^{-i2\pi x S} \langle \vec{\alpha} | e^{i2\pi x \hat{N}} e^{-i\hat{H}t} | \vec{\alpha} \rangle \\ &= e^{-\tilde{N}} \int_0^1 dx e^{-i2\pi x S} \sum_{S'=0}^{\infty} \frac{\tilde{N}^{S'}}{S'!} \langle S', \vec{\xi} | e^{i2\pi x \hat{N}} e^{-i\hat{H}t} | S', \vec{\xi} \rangle \\ &= e^{-\tilde{N}} \frac{\tilde{N}^S}{S!} \langle S, \vec{\xi} | e^{-i\hat{H}t} | S, \vec{\xi} \rangle \end{aligned} \quad (55)$$

which gives rise to the final result

$$\langle S, \vec{\xi} | e^{-i\hat{H}t} | S, \vec{\xi} \rangle = e^{\tilde{N}} \frac{S!}{\tilde{N}^S} \int_0^1 dx e^{-i2\pi x S} \langle \vec{\alpha} e^{-i2\pi x} | e^{-i\hat{H}t} | \vec{\alpha} \rangle \quad (56)$$

for the auto-correlation in complete analogy to Eq. (42). By using Stirling's formula and setting  $\tilde{N} = S$  as well as  $\alpha_1 = \alpha_2 = \dots = \sqrt{\frac{S}{M}} = \sqrt{\lambda}$ , it can be verified that Eq. (56) will reproduce the Eq. (42), which was derived for the Hamiltonian given in Eq. (18). It remains to be seen if the general relation can be applied fruitfully in the future.

## 5. Conclusions and Outlook

In the thermodynamic limit, for the interacting boson model, quantities like two-point correlation functions and the quasi-momentum distribution are the same for MMGS and GCS initial conditions. We have shown here, that for other important quantities, there exist differences between those states, even in the thermodynamic limit. To this end we have studied the quantum mechanical time-evolution of an initial wavefunction that was either a MMGS or a GCS and have proven the fact that the respective correlations are related via a Fourier-type relation. Pictorially this could be visualized via the overlap of a time evolved Gaussian with a set of other Gaussians, whose phases  $x$  are distributed along a circle with a radius that is defined by the filling factor. All those different Gaussians that by themselves are not obeying U(1) symmetry correspond to a generalized coherent state, which obeys this symmetry. The Fourier coefficient at the value  $S$  (corresponding to the fixed particle number) of the quantity  $G(x, t)$  introduced

in the main text is then shown to be the auto-correlation function of the generalized coherent state. This function is usually studied in a typical quench scenario.

Building on the Fourier relation, we could show that there are different physical reasons for the correlations to become (almost) zero and thus the free-energy density to become very large. In the thermodynamic limit, the time evolved state, by moving away from the circle, will develop zero overlap at certain instances in time and thus a diverging rate function follows, reminiscent of the case of dynamical phase transitions [29]. This connection shall be further explored in the future also for the tight-binding model with staggered onsite potential, studied previously with [38] and without external flux [28], as well as the full Bose-Hubbard model, that has thus far been studied in the context of quench dynamics using either direct numerical diagonalization [38] or matrix product state (DMRG) methods [30]. Employing generalized coherent states, a variational multi-configuration ansatz for the solution of the TDSE, along the lines of [15], is then naturally called for.

## Appendix A: Exact analytical solution for the GCS auto-correlation function

In the following, we explicitly calculate the time evolution of the GCS driven by the deep lattice, as defined in Eq. (18). Applying the time-evolution operator, we find

$$\begin{aligned}
 e^{-i\hat{H}t}|S, \vec{\xi}\rangle &= e^{-i(\sum_{i=1}^M \hat{h}_i)t} \frac{1}{\sqrt{S!}} \left( \sum_{i=1}^M \xi_i \hat{a}_i^\dagger \right)^S |\text{vac}\rangle \\
 &= \sqrt{S!} \sum_{[n_i]=S} \prod_{i=1}^M \frac{1}{n_i!} e^{-i\hat{h}_i t} (\xi_i \hat{a}_i^\dagger)^{n_i} |\text{vac}\rangle \\
 &= \sqrt{S!} \sum_{[n_i]=S} \prod_{i=1}^M \frac{1}{n_i!} (\xi_i \hat{a}_i^\dagger)^{n_i} e^{-i\frac{U}{2}(\hat{n}_i+n_i)(\hat{n}_i+n_i-1)t} |\text{vac}\rangle \\
 &= \sqrt{S!} \sum_{[n_i]=S} \prod_{i=1}^M \frac{1}{n_i!} \left[ \xi_i e^{-i\frac{U}{2}(n_i-1)t} \hat{a}_i^\dagger \right]^{n_i} |\text{vac}\rangle \\
 &= \sqrt{S!} \sum_{[n_i]=S} e^{i\frac{U}{2}St} \prod_{i=1}^M \frac{1}{n_i!} (\xi_i e^{-i\frac{U}{2}n_i t} \hat{a}_i^\dagger)^{n_i} |\text{vac}\rangle \\
 &= \sqrt{S!} \sum_{[n_i]=S} \prod_{i=1}^M \frac{1}{n_i!} (\xi_i e^{-i\frac{U}{2}n_i t} \hat{a}_i^\dagger)^{n_i} |\text{vac}\rangle, \tag{57}
 \end{aligned}$$

where in the second line we expand the GCS in terms of the Fock states as shown in Eq. (6) and apply the factors  $e^{-i\hat{h}_i t}$  to the corresponding modes. In the third line we utilize the formula

$$\hat{a}_i^\dagger f(\hat{n}_i) = f(\hat{n}_i + 1) \hat{a}_i^\dagger. \tag{58}$$

The result in the fourth line is given by the fact that

$$e^{-i\frac{U}{2}(\hat{n}_i+n_i)(\hat{n}_i+n_i-1)t} |\text{vac}\rangle = e^{-i\frac{U}{2}n_i(n_i-1)t} |\text{vac}\rangle, \tag{59}$$

and the global phase factor  $e^{i\frac{U}{2}St}$  in the second last line stems from  $e^{i\frac{U}{2}St} = \prod_{i=1}^M e^{i\frac{U}{2}n_i t}$ , which is due to that fact that the sum over all  $n_i$  gives the total number of particles, see also the text after Eq. (6).

The auto-correlation function or Loschmidt amplitude is thus finally given by

$$\langle S, \vec{\xi} | e^{-i\hat{H}t} | S, \vec{\xi} \rangle = S! \sum_{[n_i]=S} \prod_{i=1}^M \frac{|\xi_i|^{2n_i}}{n_i!} e^{-i\frac{U}{2}n_i^2 t}, \quad (60)$$

where the orthogonality of the Fock states was used.

## References

- [1] Mitra A 2018 *Annual Review of Condensed Matter Physics* **9** 245–259
- [2] Greiner M, Mandel O, Hänsch T W and Bloch I 2002 *Nature* **419** 51–54
- [3] Polkovnikov A, Sengupta K, Silva A and Vengalattore M 2011 *Rev. Mod. Phys.* **83**(3) 863–883
- [4] Trotzky S, Chen Y, Flesch A, McCulloch I P, Schollwöck U, Eisert J and Bloch I 2012 *Nat. Phys.* **8** 325
- [5] Perelomov A M 1971 *Theoretical and Mathematical Physics* **6** 156–164
- [6] Perelomov A 1986 *Generalized Coherent States and Their Applications* (Berlin: Springer-Verlag)
- [7] Arechi F T, Courtens E, Gilmore R and Thomas H 1972 *Phys. Rev. A* **6**(6) 2211–2237
- [8] Zhang W M, Feng D H and Gilmore R 1990 *Rev. Mod. Phys.* **62**(4) 867–927
- [9] Yang C N 1962 *Rev. Mod. Phys.* **34**(4) 694–704
- [10] Lieb E H, Seiringer R and Yngvason J 2007 *Reports on Mathematical Physics* **59** 389–399 ISSN 0034-4877
- [11] Schachenmayer J, Daley A J and Zoller P 2011 *Phys. Rev. A* **83**(4) 043614
- [12] Wang Z X and Heller E J 2009 *J. Phys. A* **42** 285304
- [13] Heyl M, Polkovnikov A and Kehrein S 2013 *Phys. Rev. Lett.* **110**(13) 135704
- [14] Wimberger S, Manganelli G, Brollo A and Salasnich L 2021 *Phys. Rev. A* **103**(2) 023326
- [15] Qiao Y and Grossmann F 2021 *Phys. Rev. A* **103**(4) 042209
- [16] Qiao Y and Grossmann F 2023 *Front. Phys.* **11** 1221614
- [17] Beck M, Jaeckle A, Worth G and Meyer H D 2000 *Phys. Rep.* **324** 1 – 105
- [18] Werther M and Grossmann F 2020 *Phys. Rev. B* **101** 174315
- [19] Buonsante P and Penna V 2008 *Journal of Physics A: Mathematical and Theoretical* **41** 175301
- [20] Trimborn F, Witthaut D and Korsch H J 2009 *Phys. Rev. A* **79**(1) 013608
- [21] Greiner M, Mandel O, Esslinger T, Hänsch T W and Bloch I 2002 *Nature* **415**
- [22] Glauber R J 1963 *Phys. Rev.* **131**(6) 2766–2788
- [23] Klauder J R and Skagerstam B S 1985 *Coherent States* (Singapore: World Scientific)
- [24] Werther M, Loho Choudhury S and Grossmann F 2021 *Int. Rev. in Phys. Chem.* **40** 81
- [25] Tomsovic S, Schlagheck P, Ullmo D, Urbina J D and Richter K 2018 *Phys. Rev. A* **97**(6) 061606
- [26] Dell’Anna L 2022 *Phys. Rev. A* **105**(3) 032412
- [27] Kriel J N, Karrasch C and Kehrein S 2014 *Phys. Rev. B* **90**(12) 125106
- [28] Fogarty T, Usui A, Busch T, Silva A and Goulet J 2017 *New Journal of Physics* **19** 113018
- [29] Heyl M 2018 *Reports on Progress in Physics* **81** 054001
- [30] Lacki M and Heyl M 2019 *Phys. Rev. B* **99** 121107
- [31] Wilf H S 2005 *generatingfunctionology* (CRC press)
- [32] Lindinger J 2017 *Multifractal properties of the ground state of the Bose-Hubbard model*
- [33] Jurcevic P, Shen H, Hauke P, Maier C, Brydges T, Hempel C, Lanyon B P, Heyl M, Blatt R and Roos C F 2017 *Phys. Rev. Lett.* **119**(8) 080501
- [34] Zhang J, Pagano G, Hess P W, Kyprianidis A, Becker P, Kaplan H, Gorshkov A V, Gong Z X and Monroe C 2017 *Nature* **551** 601–604

- [35] Fläschner N, Vogel D, Tarnowski M, Rem B, Lühmann D S, Heyl M, Budich J, Mathey L, Sengstock K and Weitenberg C 2018 *Nature Physics* **14** 265–268
- [36] Link V and Strunz W T 2020 *Phys. Rev. Lett.* **125**(14) 143602
- [37] Grossmann F, Rost J M and Schleich W P 1997 *J. Phys. A: Math. Gen.* **30** L277
- [38] Rossini D, Fazio R, Giovannetti V and Silva A 2014 *Europhysics Letters* **107** 30002